A co-rotational 8-node assumed strain element for large displacement elasto-plastic analysis of plates and shells

K.D. Kim†

School of Civil Engineering, Asian Institute of Technology, P.O. Box 4, Klongluang, Pathumthani, 12120, Thailand

Abstract. The formulation of a non-linear shear deformable shell element is presented for the solution of stability problems of stiffened plates and shells. The formulation of the geometrical stiffness presented here is exactly defined on the midsurface and is efficient for analyzing stability problems of thick plates and shells by incorporating bending moment and transverse shear resultant force. As a result of the explicit integration of the tangent stiffness matrix, this formulation is computationally very efficient in incremental nonlinear analysis. The element is free of both membrane and shear locking behaviour by using the assumed strain method such that the element performs very well in the thin shells. By using six degrees of freedom per node, the present element can model stiffened plate and shell structures. The formulation includes large displacement effects and elasto-plastic material behaviour. The material is assumed to be isotropic and elasto-plastic obeying Von Mises's yield condition and its associated flow rules. The results showed good agreement with references and computational efficiency.

Key words: assumed strain; co-rotational methods; analytical integration; large displacement elasto-plastic; stiffened plates and shells.

1. Introduction

With increasing emphasis on the use of the ultimate limit state design of steel structures, attention has inevitably turned to the consideration of material non-linearity as well as geometrical non-linearity. There is a lot of information available on the stability of plates and shells based on linear elastic behaviour than on the large deflection inelastic stability problem. The solutions of both geometrical and material non-linearity problems have been greatly facilitated by the development of powerful hardware and efficient formulation. In many instances numerical techniques to solve the problem for plate and shell behaviour beyond collapse have been improved. The significant effort has gone into adopting finite element techniques to solve both material and geometrically non-linear problems more accurately and efficiently. To compound the situation, in many cases, designers leap directly from the linear elastic problems to the non-linear elastoplastic problem without changing geometry on stability. The thin shell structures under in-plane loading which shows highly nonlinear effects often lose stability at much lower loads than those calculated from linear buckling analysis.

---

† Associate Professor

Thus, calculating the critical buckling load by eigenvalue analysis and tracing the equilibrium path before and after the limit load by non-linear analysis have been among the most challenging works in finite element analysis of shell structures.

Many shell element formulations have been based on the so-called 'degenerate' models introduced by Ahmad *et al*. (1970). Whilst such elements are capable of dealing with thick plate and shell problems, however their performance deteriorates rapidly as the element thickness becomes thin, which is called shear locking. The efforts by many investigators have been directed at overcoming the transverse shear locking problem in Mindlin-Reissner type element, thus making them effectively reliable for thin plate and shell applications. Javaherian and Dowling (1985) presented a semi-loop shell element for large deflection and elastoplastic analysis for thin shell analysis which ignored the transverse shear effects. Kebari and Cassell (1992) developed 9 nodes shell finite element based on a co-rotational method taking into account finite rotations respectively. In this study the shear locking is sorted out by stabilizing techniques. Kim *et al*. (1998) and Kim and Vojiadjis (1999) stated that free-of-locking behaviour in a 8 noded resultant shell element is obtained by the energy control formulation using covariant base vectors which are determined at Gauss points. For thick plate and shell elements in which the shear locking factor is greater than unity, this factor set equals to unity and the element does not require any shear locking factors. The shell finite element based on a co-rotational method is taken into account in finite rotations. The element shows very good performance in thin shells but has a spurious mode due to use of reduced integration. In order to improve the previous work by Kim *et al*. (1998), a new 8 node shell element based on the assumed strain method with the full integration is develop by Kim and Park (2001). The shell element showed very good performance compared with references using the different assumed strain methods in 8 nodes shell element by Bathe and Dvorkin (1986) and Lakshminaryana and Kailashi (1989).

The objective of this paper is to present the non-linear formulations of eight noded shell element without locking behaviour and their application to large deflection of elstoplastic analysis of steel structures.

The geometrically non-linear formulation of the shell element based on a Mindlin-Reissner theory, which assumes small strain and large displacements, is based on the updated Lagrangian method. In order to remove rigid body rotations, the co-rotational method by Bates (1987) was employed. In this method, the displacement field is referred to a set of local co-rotational co-ordinates. The polar decomposition theory was used to derive the co-rotational formulation, where the motion is decomposed into either a rigid translation followed by rigid rotation or a rigid rotation followed by rigid translation. Thus, the deformation can be isolated by removing the rigid body rotation from the total nodal displacements, which are referred to as co-rotational displacements.

In order to reduce the computational time in the incremental nonlinear analysis, the tangent stiffness matrix is formulated on the mid-surface by the analytical integration through the thickness. In this formulation the geometric stiffness matrix is further improved in comparison with volume integration done by Javaherian and Dowling (1985), Huang (1987) and Choi and Yoo (1991). Thus the computational time is significantly reduced in geometrically nonlinear analysis. By using six degrees of freedom per node, the present element can model stiffened composite plate and shell structures.

Betsch and Stein (1999) presented a large strain elasto-plasticity formulation which is suited for the implementation into assumed strain 4-noded shell elements. They used constitutive procedures based on the Cauchy-Green tensor rather than deformation gradient. The plasticity in the present is handled by applying the Von Mises yield condition and Plandtel-Reuss flow rule to discrete point
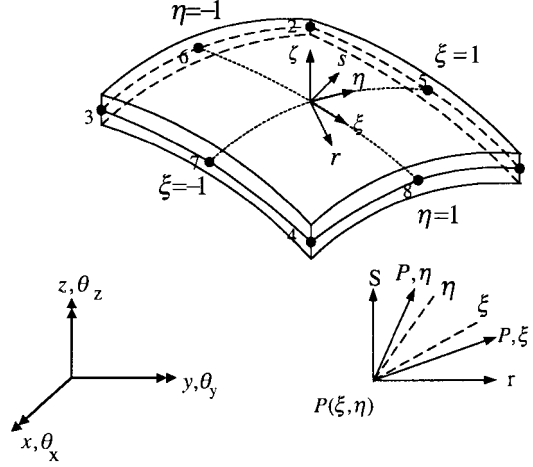
Fig. 1 Mid-surface geometry and local coordinate of 8 node shell element

through the thickness. The actual stresses components are assumed to be the plane stress components at any level of the thickness. Multi-layered approach is based on equi-spaced stations at the extreme fibers. A modified trapezoidal rule is used for the numerical integration of the constitutive relation in the plasticity part. The results of the elastoplastic analysis showed reasonably good agreement with the reference by the finite difference solution and other solution shown in the numerical examples.

2. Geometry of the shell element

The geometry of the 8-node shell element, Fig. 1, is defined by the position vector $\boldsymbol{P}$.

$$\boldsymbol{P} = \begin{Bmatrix} x \\ y \\ z \end{Bmatrix} = \sum_{i=1}^{8} H^i \boldsymbol{P}_i + t \boldsymbol{V}_t \tag{1}$$

H^i are Lagrange shape functions, $\boldsymbol{P}_i$ are nodal coordinates, $\boldsymbol{V}_t$ is unit vector normal to the shell mid-surface and t is a local coordinate in the thickness direction ranging from $-h/2$ to $h/2$.

The natural curvilinear co-ordinate is (ξ, η, ζ) and at $\zeta = 0$, the two non-dimensional coordinates ξ and η describe the shell midsurface. An orthogonal local co-ordinate (r, s, t), which rotates with the convected co-ordinates, is embedded within the element.

The base vectors $(\boldsymbol{V}_r, \boldsymbol{V}_s, \boldsymbol{V}_t)$, which are parallel to the local co-ordinates, are defined as follows:

$$\boldsymbol{V}_t = (\overline{\boldsymbol{V}}_\xi \times \overline{\boldsymbol{V}}_\eta) / \left| (\overline{\boldsymbol{V}}_\xi \times \overline{\boldsymbol{V}}_\eta) \right|$$

$$\boldsymbol{V}_s = (\boldsymbol{V}_t \times \overline{\boldsymbol{V}}_\xi + \overline{\boldsymbol{V}}_\eta) / \left| (\boldsymbol{V}_t \times \overline{\boldsymbol{V}}_\xi) + \overline{\boldsymbol{V}}_\eta \right|$$

$$\boldsymbol{V}_r = \boldsymbol{V}_s \times \boldsymbol{V}_t \tag{2}$$

where $\overline{\boldsymbol{V}}_\xi$ and $\overline{\boldsymbol{V}}_\eta$ are the unit covariant base vectors, tangent to ξ and η.

It is important to note that the coordinates r and s are not only tangential to the mid-surface but also symmetrically placed with respect to ξ and η. This is necessary in the application of the polar decomposition theorem.

Also, V_t is normal to the mid-surface of the element and it is independent of the top and the bottom nodal coordinates. This allows the assumption of ignoring the variation of the Jacobian in the thickness direction. The approximation introduced by ignoring variation of Jacobian through the thickness would not violate rigid body rotation requirement if V_t instead of V_t^i is used in the definition of the geometry of the elements.

3. Displacement field

The local incremental motion of any point of the shell is defined by the first order approximation of the Mindlin-Reissner theory. Using the transformation matrix $T = [V_r \ V_s \ V_t]$, the translations are written as

$$\Delta U = \sum_{i=1}^{8} H^i(\xi, \eta)[\Delta \overline{U}^i + t\Theta\Delta\theta^i] \tag{3}$$

where $\Delta\overline{U}^i(\Delta\overline{U}^i, \Delta\overline{V}^i, \Delta\overline{W}^i)$ and $\Delta\theta(\Delta\theta_x^i, \Delta\theta_y^i, \Delta\theta_y^i)$ are the global incremental displacement and rotation vectors which are functions of nodal values. The transformation matrix Θ has the form,

$$\Theta = \begin{bmatrix} 0 & n_t & -m_t \\ -n_t & 0 & l_t \\ m_t & -l_t & 0 \end{bmatrix} \tag{4}$$

where l_t, m_t, n_t are components of the unit vector V_t.

The traditional formulation of shell consists of first, converting global displacement values to the local coordinate system and then, are interpolated at the Gauss points. The present formulation, initiated by Kebari and Cassel (1992) first interpolates global displacement values at Gauss points and then transfer them to local coordinate. This method reduces the computational time.

4. Co-rotational displacements

The total motion of the element can be decomposed into three components, i.e., (1) a rigid translation, (2) a rigid body rotation and (3) a pure deformation. The co-rotational nodal displacement $\hat{u}$, associated with pure deformation is the remaining displacement after the removal of the rigid body motion. It is expressed as

$$\hat{u}_i = (P_i - P_{ref}) - R(\widehat{\varphi})(^0P_i - {}^0P_{ref}) . \tag{5}$$

P_i are ${}^0P_i$ the nodal position vectors P_{ref} and ${}^0P_{ref}$ are the position vectors of a reference point within the element in the current and initial configurations, respectively. $R(\widehat{\varphi})$ is the orthogonal

transformation matrix that corresponds to rigid body rotation. It relates any point with a position vector in the unconvected state $(^0r, {}^0s, {}^0t)$, to the same point with a new position vector in the convected state (r, s, t). The rotation matrix $\boldsymbol{R}(\widehat{\boldsymbol{\varphi}})$, may be obtained by

$$\boldsymbol{T} = \boldsymbol{R}(\widehat{\boldsymbol{\varphi}}) \bullet {}^0\boldsymbol{T}. \tag{6}$$

$^0\boldsymbol{T}$ and $\boldsymbol{T}$ are the transformation matrices in the initial and current configuration respectively.

A detailed discussion about the adopted finite rotation formulation is found in works of Bates (1987) and Kebari and Cassel (1992).

5. Strain-displacement relationships

The incremental Green strain tensor in local co-rotational co-ordinate system can be written as follows:

$$\Delta\hat{\varepsilon}_r = \frac{\partial\Delta\hat{u}}{\partial r} + \frac{1}{2}\left[\left(\frac{\partial\Delta\hat{u}}{\partial r}\right)^2 + \left(\frac{\partial\Delta\hat{v}}{\partial r}\right)^2 + \left(\frac{\partial\Delta\hat{w}}{\partial r}\right)^2\right]$$

$$\Delta\hat{\varepsilon}_s = \frac{\partial\Delta\hat{v}}{\partial s} + \frac{1}{2}\left[\left(\frac{\partial\Delta\hat{u}}{\partial s}\right)^2 + \left(\frac{\partial\Delta\hat{v}}{\partial s}\right)^2 + \left(\frac{\partial\Delta\hat{w}}{\partial s}\right)^2\right]$$

$$\Delta\hat{\varepsilon}_{rs} = \frac{\partial\Delta\hat{u}}{\partial s} + \frac{\partial\Delta\hat{v}}{\partial r} + \frac{\partial\Delta\hat{u}}{\partial r}\frac{\partial\Delta\hat{u}}{\partial s} + \frac{\partial\Delta\hat{v}}{\partial r}\frac{\partial\Delta\hat{v}}{\partial s} + \frac{\partial\Delta\hat{w}}{\partial r}\frac{\partial\Delta\hat{w}}{\partial s}$$

$$\Delta\hat{\varepsilon}_{rt} = \frac{\partial\Delta\hat{w}}{\partial r} + \frac{\partial\Delta\hat{u}}{\partial t} + \frac{\partial\Delta\hat{u}}{\partial r}\frac{\partial\Delta\hat{u}}{\partial t} + \frac{\partial\Delta\hat{v}}{\partial r}\frac{\partial\Delta\hat{v}}{\partial t} + \frac{\partial\Delta\hat{w}}{\partial r}\frac{\partial\Delta\hat{w}}{\partial t}$$

$$\Delta\hat{\varepsilon}_{st} = \frac{\partial\Delta\hat{w}}{\partial s} + \frac{\partial\Delta\hat{v}}{\partial t} + \frac{\partial\Delta\hat{u}}{\partial s}\frac{\partial\Delta\hat{u}}{\partial t} + \frac{\partial\Delta\hat{v}}{\partial s}\frac{\partial\Delta\hat{v}}{\partial t} + \frac{\partial\Delta\hat{w}}{\partial s}\frac{\partial\Delta\hat{w}}{\partial t} \tag{7}$$

The incremental membrane-bending strain ($\Delta\hat{\boldsymbol{\varepsilon}}_{mb}$: $\Delta\hat{\boldsymbol{\varepsilon}}_{rr}$, $\Delta\hat{\boldsymbol{\varepsilon}}_{ss}$, $\Delta\hat{\boldsymbol{\varepsilon}}_{rs}$) and transverse shear strain ($\Delta\hat{\boldsymbol{\varepsilon}}_q$: $\Delta\hat{\boldsymbol{\varepsilon}}_{rt}$, $\Delta\hat{\boldsymbol{\varepsilon}}_{st}$) can be expressed in two parts, the linear strains ($\Delta\hat{e}_{mb}$, $\Delta\hat{e}_q$) and the non-linear ($\Delta\hat{\Xi}_{mb}$, $\Delta\hat{\Xi}_q$) strains.

$$\Delta\hat{\boldsymbol{\varepsilon}}_{mb} = \Delta\hat{e}_{mb} + \Delta\hat{\Xi}_{mb}$$

$$\Delta\hat{\boldsymbol{\varepsilon}}_q = \Delta\hat{e}_q + \Delta\hat{\Xi}_q \tag{8}$$

5.1 Linear strain-displacement relationships

The linear incremental strain-displacement relations in local Cartesian orthogonal coordinate systems are given by the usual equations.

$$\Delta\hat{e}_{rr} = \frac{\partial\Delta\hat{\bar{u}}}{\partial r} + t\frac{\partial\Delta\hat{\varphi}_s}{\partial r}$$

$$\Delta\hat{e}_{ss} = \frac{\partial\Delta\hat{\bar{v}}}{\partial s} - t\frac{\partial\Delta\hat{\varphi}_r}{\partial s}$$

$$\Delta\hat{e}_{rs} = \frac{\partial\Delta\bar{v}}{\partial r} + \frac{\partial\Delta\bar{u}}{\partial s} + t\left(\frac{\partial\Delta\hat{\varphi}_s}{\partial r} - \frac{\partial\Delta\hat{\varphi}_r}{\partial s}\right)$$

$$\Delta\hat{e}_{rt} = \frac{\partial\Delta\hat{\bar{w}}}{\partial r} + \Delta\hat{\varphi}_s$$

$$\Delta\hat{e}_{st} = \frac{\partial\Delta\hat{\bar{w}}}{\partial s} - \Delta\hat{\varphi}_r \tag{9}$$

In order to express the strains in terms of nodal displacements, the local strain components are transformed to the global co-ordinates. The local displacements can be expressed in terms of local direction cosine

$$\Delta\hat{\bar{u}} = V_r^T\Delta\hat{\bar{U}}, \qquad \Delta\hat{\varphi}_s = V_s^T\Delta\hat{\boldsymbol{\theta}} \tag{10}$$

The co-rotational local strain component is then transformed in terms of global displacements,

$$\Delta\hat{e}_{rr} = \frac{\partial\Delta\hat{\bar{u}}}{\partial r} + t\frac{\partial\Delta\hat{\varphi}_s}{\partial r} = V_r^T\frac{\partial\Delta\hat{\bar{U}}}{\partial r} + tV_s^T\frac{\partial\Delta\hat{\boldsymbol{\theta}}}{\partial r} \tag{11}$$

To compute the derivative of global displacements with respect to the curvilinear system, the surface Jacobian [J], separated from thickness variation, is used. The surface Jacobian is approximately equal at all layers for reasons mentioned in Section 2.

With a similar method, each strain term being based on first order shear deformation theory, the following strain-displacement relationships are obtained.

$$\begin{Bmatrix}\Delta\hat{e}_{rr}\\\Delta\hat{e}_{ss}\\\Delta\hat{e}_{rs}\end{Bmatrix} = \sum_{i=1}^{8}\left[\begin{bmatrix}f^iV_r^T\\g^iV_s^T\\f^iV_s^T+g^iV_r^T\end{bmatrix}+t\begin{bmatrix}f^iV_s^T\\g^iV_r^T\\g^iV_s^T-f^iV_r^T\end{bmatrix}\right]\begin{Bmatrix}\Delta\hat{\bar{U}}^i\\\Delta\hat{\boldsymbol{\theta}}^i\end{Bmatrix} = \sum_{i=1}^{8}[B_m^i \; tB_b^i]\begin{Bmatrix}\Delta\hat{\bar{U}}^i\\\Delta\hat{\boldsymbol{\theta}}^i\end{Bmatrix}$$

$$\begin{Bmatrix}\Delta\hat{e}_{rt}\\\Delta\hat{e}_{st}\end{Bmatrix} = \sum_{i=1}^{8}\begin{bmatrix}f^iV_t^T & H^iV_r^T\\g^iV_t^T & -H^iV_s^T\end{bmatrix}\begin{Bmatrix}\Delta\hat{\bar{U}}^i\\\Delta\hat{\boldsymbol{\theta}}^i\end{Bmatrix} = \sum_{i=1}^{8}[B_s^i \; H_q^i]\begin{Bmatrix}\Delta\hat{\bar{U}}^i\\\Delta\hat{\boldsymbol{\theta}}^i\end{Bmatrix} \tag{12}$$

where

$$f^i = \Gamma_{11}\frac{\partial H^i}{\partial\xi} + \Gamma_{12}\frac{\partial H^i}{\partial\eta}$$

$$g^i = \Gamma_{21}\frac{\partial H^i}{\partial\xi} + \Gamma_{22}\frac{\partial H^i}{\partial\eta} \tag{13}$$

and Γ_{11}, Γ_{12}, Γ_{21} and Γ_{22} are components of the inverse of the Jacobian matrix.

The above equation can be expressed as compact forms,

$$\Delta\hat{\boldsymbol{e}}_m = \sum_{i=1}^{8} \boldsymbol{B}_m^i \Delta\hat{\bar{\boldsymbol{U}}}^i$$

$$\Delta\hat{\boldsymbol{e}}_b = \sum_{i=1}^{8} \boldsymbol{B}_b^i \Delta\hat{\boldsymbol{\theta}}^i$$

$$\Delta\hat{\boldsymbol{e}}_q = \sum_{i=1}^{8} [\boldsymbol{B}_q^i \ \boldsymbol{H}_q^i] \left\{ \begin{array}{c} \Delta\hat{\bar{\boldsymbol{U}}}^i \\ \Delta\hat{\boldsymbol{\theta}}^i \end{array} \right\} \tag{14}$$

$\boldsymbol{B}_m^i$, $\boldsymbol{B}_b^i$ and $[\boldsymbol{B}_q^i \ \boldsymbol{H}_q^i]$ are the strain-displacement matrices due to membrane, bending and transverse shear, respectively.

5.2 Transverse shear and membrane locking

In order to avoid locking problems, the assumed natural strain method in the linear shell element by Kim and Park (2002) is extended to the nonlinear shell element. Thus the transverse shear and membrane strain fields are interpolated with the following sampling points in Fig. 2.

The interpolation function for assumed natural strain is shown in the following Table 1.

5.3 Non-linear strain displacement relation

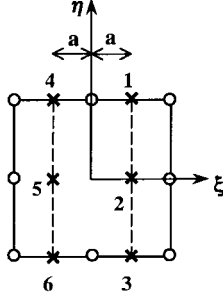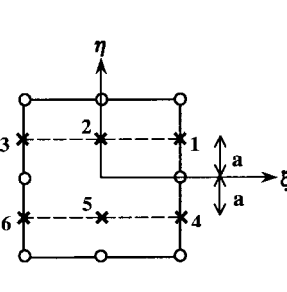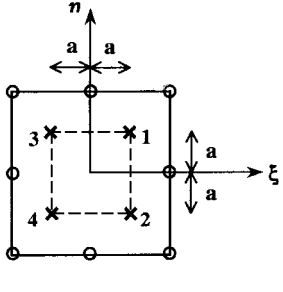In order to derive the geometric stiffness matrix, the non-linear part of incremetal Green strain

Sampling points and coefficients of $\tilde{\boldsymbol{B}}$ matrix related to strains $\tilde{e}_{rr}$, $\tilde{\gamma}_{rt}$ $a = 1/\sqrt{3}$	Sampling points and coefficients of $\tilde{\boldsymbol{B}}$ matrix related to strains $\tilde{e}_{ss}$, $\tilde{\gamma}_{st}$ $a = 1/\sqrt{3}$	Sampling points and coefficients of $\tilde{\boldsymbol{B}}$ matrix related to strain $\tilde{e}_{rs}$ $a = 1/\sqrt{3}$

Fig. 2 Sampling points

Table 1 Interpolation function for assumed natural strain fields

$\tilde{H}^i$	*Two point interpolation functions - P_i, P_j	*Three point interpolation functions - Q_j
1) $\displaystyle\sum_{i=1}^{2}\sum_{j=1}^{3} P_i(\xi)Q_j(\eta)$		$Q_1(\eta) = \frac{1}{2}\eta(\eta+1)$
	$P_1(\xi) = \frac{1}{2}(1+\sqrt{3}\xi)$	
2) $\displaystyle\sum_{i=1}^{2}\sum_{j=1}^{3} P_i(\eta)Q_j(\xi)$		$Q_2(\eta) = 1-\eta^2$
	$P_2(\xi) = \frac{1}{2}(1+\sqrt{3}\xi)$	
3) $\displaystyle\sum_{i=1}^{2}\sum_{j=1}^{3} P_i(\xi)P_j(\eta)$		$Q_3(\eta) = \frac{1}{2}\eta(\eta-1)$

*$P(\eta)$ and $Q(\xi)$ can be obtained by changing variables.

tensor in local coordinate system could be expressed as the global coodinates.

$$\Delta\hat{\boldsymbol{\Xi}} = \frac{1}{2}\begin{bmatrix} \dfrac{\partial\Delta\hat{\boldsymbol{u}}^T}{\partial r} & 0 & 0 \\[2mm] 0 & \dfrac{\partial\Delta\hat{\boldsymbol{u}}^T}{\partial s} & 0 \\[2mm] \dfrac{\partial\Delta\hat{\boldsymbol{u}}^T}{\partial s} & \dfrac{\partial\Delta\hat{\boldsymbol{u}}^T}{\partial r} & 0 \\[2mm] \dfrac{\partial\Delta\hat{\boldsymbol{u}}^T}{\partial t} & 0 & \dfrac{\partial\Delta\hat{\boldsymbol{u}}^T}{\partial r} \\[2mm] 0 & \dfrac{\partial\Delta\hat{\boldsymbol{u}}^T}{\partial t} & \dfrac{\partial\Delta\hat{\boldsymbol{u}}^T}{\partial s} \end{bmatrix}\begin{bmatrix} \dfrac{\partial\Delta\hat{\boldsymbol{u}}}{\partial r} \\[2mm] \dfrac{\partial\Delta\hat{\boldsymbol{u}}}{\partial s} \\[2mm] \dfrac{\partial\Delta\hat{\boldsymbol{u}}}{\partial t} \end{bmatrix} = \frac{1}{2}\Delta\boldsymbol{Q}\Delta\boldsymbol{\Omega} \tag{16}$$

and the variation of $\Delta\hat{\boldsymbol{\Xi}}$ is as follows:

$$\delta(\Delta\hat{\boldsymbol{\Xi}}) = \Delta\boldsymbol{Q}\,\delta(\Delta\boldsymbol{\Omega}) = \delta(\Delta\boldsymbol{Q})\Delta\boldsymbol{\Omega} \tag{17}$$

The each component of displacement gradient can be expressed as follows:

$$\frac{\partial\hat{\boldsymbol{u}}}{\partial r} = \begin{Bmatrix} \dfrac{\partial\hat{u}}{\partial r} \\[2mm] \dfrac{\partial\hat{v}}{\partial r} \\[2mm] \dfrac{\partial\hat{w}}{\partial r} \end{Bmatrix} = \sum_{i=1}^{8}\begin{Bmatrix} f^i\boldsymbol{V}_r^T \\ f^i\boldsymbol{V}_s^T \\ f^i\boldsymbol{V}_t^T \end{Bmatrix}\{\hat{\bar{\boldsymbol{U}}}^i\} + t\sum_{i=1}^{8}\begin{Bmatrix} f^i\boldsymbol{V}_s^T \\ -f^i\boldsymbol{V}_r^T \\ \boldsymbol{0} \end{Bmatrix}\{\hat{\boldsymbol{\theta}}^i\}$$

$$= \sum_{i=1}^{8}(\boldsymbol{G}_1^i\,\hat{\bar{\boldsymbol{U}}}^i + t\boldsymbol{G}_2^i\hat{\boldsymbol{\theta}}^i) \tag{18}$$

Similarly the other terms are as follows:

$$\frac{\partial \hat{\boldsymbol{u}}}{\partial s} = \sum_{i=1}^{8} (\boldsymbol{G}_3^i \hat{\overline{\boldsymbol{U}}}^i + t\boldsymbol{G}_4^i \hat{\boldsymbol{\theta}}^i) \tag{19}$$

$$\frac{\partial \hat{\boldsymbol{u}}}{\partial t} = \sum_{i=1}^{8} \boldsymbol{G}_5^i \hat{\boldsymbol{\theta}}^i \tag{20}$$

The incremental gradient displacement ($\boldsymbol{\Omega}$) for non-linear part is interpolated from the nodal displacement.

$$\Delta\boldsymbol{\Omega} = \begin{bmatrix} \dfrac{\partial \Delta \hat{\boldsymbol{u}}}{\partial r} \\[2mm] \dfrac{\partial \Delta \hat{\boldsymbol{u}}}{\partial s} \\[2mm] \dfrac{\partial \Delta \hat{\boldsymbol{u}}}{\partial t} \end{bmatrix} = \sum_{i=1}^{8} \begin{bmatrix} \boldsymbol{G}_1^i & t\boldsymbol{G}_2^i \\ \boldsymbol{G}_3^i & t\boldsymbol{G}_4^i \\ 0 & \boldsymbol{G}_5^i \end{bmatrix} \begin{Bmatrix} \Delta\hat{\overline{\boldsymbol{U}}}^i \\ \Delta\hat{\boldsymbol{\theta}}^i \end{Bmatrix}$$

$$= \boldsymbol{G}\Delta\hat{\boldsymbol{U}} \tag{21}$$

Then incremental variation of the non-linear part of Green strain is as follows:

$$\boldsymbol{\delta}(\Delta\hat{\boldsymbol{\Xi}}) = (\Delta\boldsymbol{Q})\boldsymbol{G}\boldsymbol{\delta}(\Delta\hat{\boldsymbol{U}}) \tag{22}$$

6. Constitutive relation

The incremental constitutive law for elasto-plastic material is expressed as follows:

$$\begin{Bmatrix} \Delta\sigma_r \\ \Delta\sigma_s \\ \Delta\sigma_{rs} \end{Bmatrix} = \begin{bmatrix} C_{11} & C_{12} & C_{13} \\ C_{21} & C_{22} & C_{23} \\ C_{31} & C_{32} & C_{33} \end{bmatrix} \begin{Bmatrix} \Delta\hat{e}_r \\ \Delta\hat{e}_s \\ \Delta\hat{e}_{rs} \end{Bmatrix} = \boldsymbol{C}_{ep}\Delta\hat{\boldsymbol{e}}_{mb}$$

$$\begin{Bmatrix} \Delta\sigma_{rt} \\ \Delta\sigma_{st} \end{Bmatrix} = \frac{5}{6}\begin{bmatrix} G & 0 \\ 0 & G \end{bmatrix} \begin{Bmatrix} \Delta\hat{e}_{rt} \\ \Delta\hat{e}_{st} \end{Bmatrix} = \boldsymbol{C}_q\Delta\hat{\boldsymbol{e}}_q \tag{23}$$

In co-rotational approach the membrane-bending strain $\Delta\hat{\boldsymbol{e}}_{mb}$ is taken as the difference between the corotational strains in the current configuration and the corotational strain in the next configuration. This definition allows a path independent, Euler forward integration scheme, to be used. The corotational strain increments can be directly transformed to Cauchy stress increments without recourse to expensive transformation.

The constitutive law will be based on the Von Mises yield function and Prandtl-Reuss flow rule. The yield function has the form

$$F = \overline{\sigma} - \sigma_Y(\overline{h}) = 0 \tag{24}$$

where $\bar{\sigma}$ is effective stress and σ_Y, $\bar{h}$ are the current uni-axial yield stress and hardening parameter respectively. In the present case, the model is assumed to be limited to linear isotropic hardening, thus the relationship between the equivalent uniaxial stress and strain takes the bilinear form.

The quantity $\bar{\sigma}$ and $\bar{h}$ in Eq. (24) are defined as follows:

$$\bar{\sigma} = (\sigma_r^2 + \sigma_s^2 - 2\sigma_r\sigma_s + 3\sigma_{rs}^2)^{1/2}$$

$$\bar{h} = E_p/(1 - E_p/E) \tag{25}$$

where E_p is strain hardening parameter.

An explicit form of C_{ep} can be derived from the definition

$$C_{ep} = C_e - \frac{C_e \boldsymbol{f}\boldsymbol{f}^T C_e}{\bar{h} + \boldsymbol{f}^T C_e \boldsymbol{f}} \tag{26}$$

where C_e is the elastic constitutive coefficient and flow vector $\boldsymbol{f}$

$$C_e = \frac{E}{1-v^2}\begin{bmatrix} 1 & v & 0 \\ v & 1 & 0 \\ 0 & 0 & \dfrac{1-v}{2} \end{bmatrix} \tag{27}$$

$$\boldsymbol{f} = [\partial\bar{\sigma}/\partial\sigma_r, \ \partial\bar{\sigma}/\partial\sigma_s, \ \partial\bar{\sigma}/\partial\sigma_{rs}] \tag{28}$$

Introducing the deviatoric stress $(\sigma_r', \sigma_s', \sigma_{rs}')$ components

$$\sigma_r' = 1/3(2\sigma_r - \sigma_{sr})$$
$$\sigma_s' = 1/3(2\sigma_s - \sigma_r)$$
$$\sigma_t' = -1/3(2\sigma_r + \sigma_{sr})$$
$$\sigma_{rs}' = \sigma_{sr} \tag{29}$$

Flow vector $(\boldsymbol{f})$ can be written as follows:

$$\boldsymbol{f} = \frac{3}{2}\bar{\sigma}[\sigma_r', \sigma_r', \sigma_{rs}'] \tag{30}$$

Substituting Eqs. (29) and (30) into Eq. (26) leads to an explicit definition of C_{ep}, i.e.,

$$C_{ep} = \frac{2G}{\bar{h}}\begin{bmatrix} a - a_r^2 - \sigma_r'^2, & b - a_r a_s - \sigma_s'\sigma_r', & a_r a_{rs} - \sigma_r'\sigma_{rs}' \\ & a - a_s^2 - \sigma_s'^2 & a_s a_{rs} - \sigma_s'\sigma_{rs}' \\ \text{Symmetric} & & \dfrac{\bar{h}}{2} - a_{rs}^2 - \sigma_{rs}'^2 \end{bmatrix} \tag{31}$$

where

$$\bar{h} = 2/3\bar{\sigma}^2(1 + \bar{h}/3G)$$
$$a = \bar{h}(1 - v)/(1 - 2v)$$
$$b = \bar{h}v/(1 - 2v)$$
$$c = \sqrt{a - \sigma_t^2}$$
$$a_r = (b - \sigma_r' \sigma_t')/c$$
$$a_s = (b - \sigma_s' \sigma_s')/c$$
$$a_{rs} = \sigma_t'\sigma_{rs}'/c \tag{32}$$

Elastic unloading of material that has previously been loaded into the plastic range, can be detected by finding equivalent plastic strain increment $\Delta\bar{e}_p$.

$$\Delta\bar{e}_p = \left(\frac{C_e f f^T C_e}{\bar{h} + f^T C_e f}\right)\Delta\hat{e}_{mb} \tag{33}$$

Introducing the definitions (26) and (27) leads to the more convenient form.

$$\Delta\bar{e}_p = \frac{2\bar{\sigma}}{3(g^T\Delta\hat{e}_{mb})} \frac{1}{\frac{2\bar{h}}{9G}(1 - v)\bar{\sigma}^2 + f^T g} \tag{34}$$

where

$$g = [\sigma_r' + v\sigma_s', \sigma_s' + v\sigma_r', (1 - v)\sigma_{rt}'] \tag{35}$$

During unloading from a plastic state $\Delta e_p < 0$ whereas during conditions of plastic flow $\Delta e_p \geq 0$.

The stress increments $\Delta\boldsymbol{\sigma}$ can evidently be found using the elastoplastic constitutive matrix C_{ep}. However, a more efficient method can be derived by decomposing Δe into elastic and plastic parts Δe_e and Δe_p respectively. Then

$$\Delta\boldsymbol{\sigma} = C_e\Delta e_e = C_e(\Delta\hat{e}_{mb} - \Delta e_p) \tag{36}$$

where $\Delta e_p = \Delta\bar{e}_p f$.

In the foregoing derivation, it was tacitly assumed that Δe are increments of elastoplastic strain, i.e., that the material had already been loaded into the plastic range at the beginning of the increment. In practice, a method of calculating the portion of Δe that corresponds to elastic straining, during the transition from elastic to plastic behaviour, is required.

Let this portion be $\tilde{r}$, the stress state corresponding to the initiation of elastoplastic straining is then given by

$$\boldsymbol{\sigma} \Rightarrow \boldsymbol{\sigma} + \tilde{r}\boldsymbol{\sigma} \tag{37}$$

The elastoplastic increments are

$$\Delta\hat{e}_{mb} \Rightarrow (1 - \tilde{r})\Delta\hat{e}_{mb} \tag{38}$$

where the symbol $\Rightarrow$ denotes replacement.

Since the elastoplastic strain increments $\Delta\hat{e}_{mb}$ are finite, the calculated stress state at the end of the current step will not lie on the yield surface. However, by dividing $\Delta\hat{e}_{mb}$ into a suitable number of subincrements, and applying Eq. (36) the error can be greatly reduced. During this process, there will be a tendency for the stress state to drift away from the yield surface, but this effect can easily be eliminated by moving back to the surface at the end of each subincremental step. For this purpose, the so called "radial return" method can be used, i.e.,

$$\boldsymbol{\sigma} \Rightarrow \left(\frac{\sigma_y}{\bar{\boldsymbol{\sigma}}}\right)\boldsymbol{\sigma} \tag{39}$$

Because subincremental calculation is expensive, it is recommended that the number of subincrements to be used in any given case should be calculated automatically. In this respect, it is worth noting that the conventional approach of basing the number of subincrements purely on the excess stress, is rather crude $\bar{\boldsymbol{\sigma}} - \sigma_y$.

7. Stress resultants and tangential rigidity

The shell element displays resultant membrane forces, moments and transverse shear forces, shown in Fig. 3, obtained by integration of stresses through the thickness.

$$\left\{ \begin{array}{c} \Delta\boldsymbol{R}_{mb} \\ \Delta\boldsymbol{R}_q \end{array} \right\} = \begin{bmatrix} \boldsymbol{D}_{mb} & 0 \\ 0 & \boldsymbol{D}_q \end{bmatrix} \left\{ \begin{array}{c} \Delta\hat{e}_{mb} \\ \Delta\hat{e}_q \end{array} \right\} \tag{40}$$

where $\boldsymbol{R}_{mb} = \{N_r, N_s, N_{rs}, M_r, M_s, M_{rs}\}$ and $\boldsymbol{R}_q = \{Q_r, Q_s\}$.

The actual behaviour of transverse shear strain has parabolic distribution through the thickness. In accordance with the Mindlin-Reissner theory, the transverse shear strain is assumed as a constant distribution through the wall.

The compact incremental stress resultants ($\boldsymbol{R}$) and strains are related by elasto-plastic rigidity matrix $\boldsymbol{D}_{ep}$, i.e.,

$$\Delta\boldsymbol{R} = \boldsymbol{D}_{ep}\Delta\hat{e} \tag{41}$$

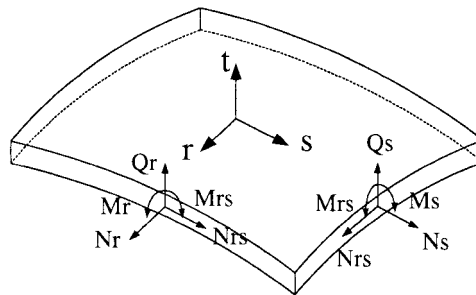The membrane-bending $\boldsymbol{D}_{mb}$ and shear strain rigidity $\boldsymbol{D}_s$ have 6×6 and 2×2 matrix respectively.

Fig. 3 Stress resultants of shell element

$$D_{mb} = \int_{-2/h}^{2/h} \begin{bmatrix} C_{ep} & tC_{ep} \\ tC_{ep} & t^2C_{ep} \end{bmatrix} dt \qquad (42)$$

$$D_q = \frac{5}{6}h \begin{bmatrix} G & 0 \\ 0 & G \end{bmatrix} \qquad (43)$$

when the entire cross section is isotropic elastic then the rigidity matrix reduces to the following form.

$$D_e = \begin{bmatrix} hC_e & 0 & 0 \\ 0 & \frac{h^3}{12}C_e & 0 \\ 0 & 0 & hC_q \end{bmatrix} \qquad (44)$$

where C_e and C_q are the elastic constitutive coefficient of membrane-bending and transverse shear part.

In order to incorporate the nonlinear material behaviour, integration of Eq. (42) must evidently be carried out numerically. Because the yield function is convex, the mid-ordinate and trapezoidal rules lead to lower and upper bound results. The Newton-Cotes formulae are based on a least-square polynomial fit, and, although accurate for smooth function, they are generally less reliable than the mid-ordinate or trapezoidal rules for piecewise functions. Gauss quadrature suffers from the same disadvantage as Newton-Cotes method. In addition, it has the drawback of being based on irregularly spaced stations none of which lie at the extreme fibres. Against this background, it makes good sense to introduce an alternative quadrature scheme that is more accurate than the mid-ordinate or trapezoidal rules for discontinuous functions, and yet can maintain a comparable accuracy to the Newton-Cotes rule for smooth functions.

This objective can be met with sufficient precision by modifying the standard (composite) trapezoidal rule so that it will exactly integrate a piecewise quadratic function of the Form $F(t^2) = f(t)g(t)$ where $f(t)$ and $g(t)$ are linear and piecewise linear functions of t respectively. The resulting rules can be written as

$$I = \Delta t/2 \left\{ (f_i + \Delta f/3)g_1 + 2\sum_{i=2}^{n-1} f_i g_i + (f_n - \Delta f/3)g_n \right\} \qquad (43)$$

where $\Delta t = h/(n-1)$, $\Delta f = (f_n - f_i)/(n-1)$ and n is the number of equi-spaced stations through the depth $(-h/2 \le t \le h/2)$. The beauty of the rule is that, compared to the standard form, the truncation error is reduced from $o(\Delta t^2)$ to $o(\Delta t^3)$, without any increase in the number of stations. Furthermore, the basic form of the trapezoidal rule is preserved, the only change being a shift in the function $f(t)$ for the first and last stations. The description in detail is found in reference by Bates (1987).

In the present case, all terms appearing in Eq. (42) takes one of the following forms:

$$I_1 = \int_{-h/2}^{h/2} g(t)dt, \qquad I_2 = \int_{-h/2}^{h/2} tg(t)dt, \qquad I_3 = \int_{-h/2}^{h/2} t^2 g(t)dt \qquad (44)$$

Applying Eq. (43) to each form in turn results in

$$I_1 = \Delta t/2 \left[g_1 + 2\sum_{i=2}^{n-1} g_i + g_n \right]$$

$$I_2 = \Delta t/2 \left[(t_1 + \Delta t/3)g_1 + 2\sum_{i=2}^{n-1} t_i g_i + (t_n - \Delta t/3)g_n \right]$$

$$I_3 = \Delta t/2 \left[(t_1 + \Delta t/3)t_1 g_1 + 2\sum_{i=2}^{n-1} t_i g_i + (t_n - \Delta t/3)t_1 g_n \right] \tag{45}$$

8. Incremental equation of equilibrium

At large strain the generalized Hook's law does not represent an approximate material behaviour description because stress-strain relation is non-linear. In practice Hook's law is only applicable to small strain, which constitutive tensor is constant coefficient. Belytschko and Hsieh (1973) showed that the total co-rotational strain can be obtained from the linear strain displacement relations in case of small strain.

Using small strain assumption, the following incremental equilibrium equation in co-rotational co-ordinate system is obtained.

$$\int \delta(\Delta\hat{e})^T C \Delta\hat{e} \, dV + \int \sigma \delta(\Delta\hat{\Xi}) \, dV = {}^{t+\Delta t}\delta W_{ex} - \int \delta(\Delta\hat{e})^T \sigma \, dV \tag{46}$$

where superscript t which is generally used as the current configuration is ignored in the above Eq. (46) and superscript $t + \Delta t$ is the adjust incremented configuration, ${}^{t+\Delta t}\delta W_{ex}$ is the external virtual work in $t + \Delta t$.

9. Element stiffness matrices

The total tangent stiffness comprises the material stiffness and the geometric stiffness matrix. The linear part of the Green strain tensor is used to derive the material stiffness matrix and non-linear part of the Green strain tensor is used to derive the geometric stiffness matrix.

9.1 Material stiffness matrix

If the strain-displacement Eq. (14) is substituted into Eq. (46), the linearized element material stiffness matrix (K_M^e) is obtained.

$$\int \delta(\Delta\hat{e})^T C_{ep} \Delta\hat{e} \, dV = \delta\Delta\hat{U}^T (\int B^T C_{ep} B \, dV)\hat{U} = \delta\Delta\hat{U}^T K_M^e \Delta\hat{U} \tag{47}$$

i.e.,

$$\boldsymbol{K}_M^e = \int_v (\boldsymbol{B})^T \boldsymbol{C}_{ep} \boldsymbol{B} \, dV$$

$$= \int_s \int_{-h/2}^{h/2} \begin{bmatrix} (\boldsymbol{B}_m^i)^T \boldsymbol{C}_{ep} \boldsymbol{B}_m^j + (\boldsymbol{B}_q^i)^T \boldsymbol{C}_q \boldsymbol{B}_q^j, & (\boldsymbol{B}_m^i)^T (t\boldsymbol{C}_{ep}) \boldsymbol{B}_b^j + (\boldsymbol{B}_q^i)^T \boldsymbol{C}_q \boldsymbol{H}_q^j \\ (\boldsymbol{B}_b^i)^T (t\boldsymbol{C}_{ep}) \boldsymbol{B}_m^j + (\boldsymbol{H}_q^i)^T \boldsymbol{C}_q \boldsymbol{B}_q^j, & (\boldsymbol{B}_b^i)^T (t^2 \boldsymbol{C}_{ep}) \boldsymbol{B}_b^j + (\boldsymbol{H}_q^i)^T \boldsymbol{C}_q \boldsymbol{H}_q^j \end{bmatrix}^T dt dS \quad (48)$$

where i and j range from 1 to the number of nodes and the derivation of the sub component is straightforward. The element stiffness matrix is analytically integrated through the thickness and for the laminate composite rigidity is integrated over each layer. Finally the element stiffness matrix has 6×6 size on the reference-surface of shell (S).

To model stiffened plates and shells, the need for six degrees of freedom arises because the process of stiffness accumulation at any node lying on the junction must be carried out in a single reference frame. The two constraint stiffness matrices are found in reference by Kim and Park (2001).

9.2 Geometric stiffness matrix

Structures composed of plates and shells are stiff in in-plane deformation but flexible in bending deformations. In the stability analysis of thin shells, the effect of membrane and bending strains must be included. The effect of transverse shear deformation in the nonlinear analysis of thick shell is also required in the formulation of geometric stiffness. Ziegler (1968) showed that presence of transverse shear decreases the buckling load of an isotropic beam. The following geometric stiffness formulation is developed to incorporate the membrane-bending and transverse shear forces on the reference surface and it can be compared with formulation based on Von-Karman theory suitable for thin plate and shell stability.

In order to formulate geometric stiffness matrix accurately, the stress values should be evaluated accurately. The accuracy of the computation of stresses for formulation of geometric stiffness matrix is maintained by obtaining the same interpolated strains in the computation of linear stiffness matrix. The stresses are computed at the integration points based on these strains.

Substituting the non-linear part of strain (16) into Eq. (46), the following geometric stiffness matrix is obtained.

$$\int \boldsymbol{\sigma} \delta(\Delta \hat{\boldsymbol{\Xi}}) dV = \int \delta(\Delta \hat{\boldsymbol{\Xi}})^T \boldsymbol{\sigma} \, dV = \int \delta \Delta \boldsymbol{\Omega}^T \Delta \boldsymbol{Q}^T \boldsymbol{\sigma} \, dV \quad (49)$$

Then,

$$\Delta \boldsymbol{Q}^T \boldsymbol{\sigma} = \begin{bmatrix} \sigma_r \boldsymbol{I}_3 & \sigma_{rs} \boldsymbol{I}_3 & \sigma_{rt} \boldsymbol{I}_3 \\ \sigma_{rs} \boldsymbol{I}_3 & \sigma_s \boldsymbol{I}_3 & \sigma_{st} \boldsymbol{I}_3 \\ \sigma_{rt} \boldsymbol{I}_3 & \sigma_{st} \boldsymbol{I}_3 & 0 \end{bmatrix} \Delta \boldsymbol{\Omega} = \boldsymbol{S} \boldsymbol{G} \Delta \hat{\boldsymbol{U}} \quad (50)$$

in which $\boldsymbol{I}_3$ is a 3×3 identity matrix. Using mechanics of material theory and substituting Eq. (50) into Eq. (49) yields

$$\int \boldsymbol{\sigma} \delta(\Delta \hat{\boldsymbol{\Xi}}) dV = \int \delta \Delta \boldsymbol{\Omega}^T \boldsymbol{S} \boldsymbol{G} \Delta \hat{\boldsymbol{U}} \, dV = \delta \Delta \hat{\boldsymbol{U}}^T \int \boldsymbol{G}^T \boldsymbol{S} \boldsymbol{G} \, dV \Delta \hat{\boldsymbol{U}} = \delta \Delta \hat{\boldsymbol{U}}^T \boldsymbol{K}_G^e \Delta \hat{\boldsymbol{U}} \quad (51)$$

i.e.,

$$\boldsymbol{K}_G^e = \int \boldsymbol{G}^T S \boldsymbol{G} dV$$

$$= \int_S \int_{-h/2}^{h/2} \begin{bmatrix} \boldsymbol{G}_1^{iT} & \boldsymbol{G}_3^{iT} & \boldsymbol{0} \\ t\boldsymbol{G}_2^{iT} & t\boldsymbol{G}_4^{iT} & \boldsymbol{G}_5^{iT} \end{bmatrix} \begin{bmatrix} \left(\dfrac{N_r}{h}+12\dfrac{M_r}{h^3}t\right)\boldsymbol{I}_3 & \left(\dfrac{N_{rs}}{h}+12\dfrac{M_{rs}}{h^3}t\right)\boldsymbol{I}_3 & \left(\dfrac{3Q_r}{2h}-6\dfrac{Q_r}{h^3}t^2\right)\boldsymbol{I}_3 \\ & \left(\dfrac{N_s}{h}+12\dfrac{M_{rs}}{h^3}t\right)\boldsymbol{I}_3 & \left(\dfrac{3Q_s}{2h}-6\dfrac{Q_s}{h^3}t^2\right)\boldsymbol{I}_3 \\ \text{Symmetric} & & 0 \end{bmatrix} \begin{bmatrix} \boldsymbol{G}_1^i & t\boldsymbol{G}_2^i \\ \boldsymbol{G}_3^i & t\boldsymbol{G}_4^i \\ 0 & \boldsymbol{G}_5^i \end{bmatrix} dt dS \quad (52)$$

The geometric stiffness matrix in Eq. (52) in the local co-rotational coordinate is analytically integrated through the thickness. By the transformation to the global frame the element geometric stiffness matrix is obtained on the global frame with 6×6 sub matrix. The following geometric stiffness with the stress resultant form can be compared with the geometric stiffness formulated by Yoo and Choi (2000).

$$[K^e]_G^{ij} = \int \begin{bmatrix} K_{11}^e & K_{12}^e \\ K_{21}^e & K_{22}^e \end{bmatrix}_G^{ij} dS \quad (53)$$

where subcomponent of the geometric stiffness (53) is as follows:

$$[K_{11}^e]_G^{ij} = \{f^i(N_r f^j + N_{rs} g^j) + g^i(N_s g^j + N_{rs} f^j)\}\boldsymbol{I}_3$$

$$[K_{12}^e]_G^{ij} = \{f^i(M_r f^j + M_{rs} g^j) + g^i(M_s g^j + M_{rs} f^j) + N^i(Q_r f^j + Q_s g^j)\}\boldsymbol{\Theta}$$

$$[K_{21}^e]_G^{ij} = \{f^i(M_r f^j + M_{rs} g^j) + g^i(M_s g^j + M_{rs} f^j) + N^j(Q_r f^i + Q_s g^i)\}\boldsymbol{\Theta}^T$$

$$[K_{22}^e]_G^{ij} = \left\{\frac{h^2}{12}f^i(N_r f^j + N_{rs} g^j) + g^i(N_s g^j + N_{rs} f^j)\right\}\boldsymbol{\Phi} \quad (54)$$

$\boldsymbol{\Theta}$ is defined in the Eq. (4) and $\boldsymbol{\Phi}$ is defined in the following equation.

$$\boldsymbol{\Phi} = \begin{bmatrix} l_s^2 + l_r^2 & l_s m_s + l_r m_r & l_s n_s + l_r n_r \\ l_s m_s + l_r m_r & m_s^2 + m_r^2 & m_s n_s + m_r n_r \\ l_s n_s + n_r l_r & n_s m_s + n_r m_r & n_s^2 + n_r^2 \end{bmatrix} \quad (55)$$

It is worth noting that, if the von Karman approximation is used, then $[K_{12}^e]_G^{ij}$, $[K_{21}^e]_G^{ij}$ and $[K_{22}^e]_G^{ij}$ vanishes and geometric stiffness is a function of the in-plane stress resultants only. However, the von Karman approximation is only suitable for thin plates and shells in which the effects of transverse shear deformation can be ignored. The above geometric stiffness matrix includes of the membrane, bending and the transverse shear forces and gives the complete definition. The geometric stiffness can be compared with the geometric stiffness formulated by Yoo and Choi (2000).

10. Internal and external forces

Let the virtual displacement at the node be $\delta\Delta U^e$. The work done by the nodal forces is equal to the sum of the products of the individual force components and corresponding displacements, i.e., in matrix form

$$^{t+\Delta t}\delta W_{ex} = \delta\Delta U^T\ {}^{t+\Delta t}P^e \tag{56}$$

The nodal forces that are in equilibrium with internal stresses for an element are

$$\int\delta(\Delta\hat{e})^T\sigma dV = \delta\Delta\hat{U}^T F^e \tag{57}$$

The internal force vector yields

$$\{F^i\}^e = \int(B^i)^T R dS \tag{58}$$

where B^i is the linear operator matrix and R is the vector of internal stress resultant.

11. Postbuckling analysis

In non-linear solution, solving for the total displacement, the translation is updated by the additive relation and the rotation matrix is updated by spectral analysis.

$$^{t+\Delta t}\hat{\overline{U}} \Rightarrow {}^{t}\hat{\overline{U}} + \Delta{}^{t}\hat{\overline{U}}$$

$$^{t+\Delta t}\hat{R}(\theta) \Rightarrow {}^{t}R(\Delta\theta){}^{t}R(\theta) \tag{59}$$

Based on the Eq. (46), the incremental non-linear equilibrium equation can be written as.

$$\delta\Delta\hat{U}^T(K_M^e + K_G^e)\Delta\hat{U} = \delta\Delta\hat{U}^T({}^{t+\Delta t}P^e - F^e) \tag{60}$$

Then the final assembled incremental non-linear equilibrium equation can be written as

$$(K_M + K_G)\Delta\hat{U} = {}^{t+\Delta t}P - F \tag{61}$$

where P and F are the external and internal forces respectively.

The equilibrium equation must be satisfied throughout the complete history of loading and the non-linear processing will be stopped only when the out of balance forces are negligible within a certain convergence limit. If it is necessary to extend the stability analysis beyond the limit point, i.e., in the so-called post-buckling range, appropriate solution procedures must be applied. One approach is to use the arc-length control method in conjunction with Newton-Raphson method to extend the stability analysis beyond the limit point by Crisfield (1981).

12. Numerical example

The general purpose package (**FINAS**) which is suitable for the nonlinear analysis of thin-walled structures on the UNIX environment was developed in Imperial college, London (1990). Based on this **FINAS**, the e**X**tended version of **FINAS** (**XFINAS**) for the non-linear dynamic analysis has

been developed on the Window 2000 Operating System in AIT. The program is particularly suited to structural dynamic stability problems and has been used extensively in the modeling of thin-walled structures. The finite element analysis was undertaken using a general purpose Non-linear Dynamic Finite Element Package (**XFINAS**).

To demonstrate the capability of the shell element and to identify its limitation, a variety of linear and non-linear problems were tested. The results of the linear analysis of the present shell element by Kim and Park (2001) showed very good agreement with references. In the following several examples are given to demonstrate the efficiency and accuracy of the present nonlinear shell element.

12.1 Morley hemispherical shell with 18° hole problem

MacNeal and Harder (1985) proposed the hemispherical shell problem for the validation of shell elements, which is shown in Fig. 4. The results are shown in Table 2. The value of the displacement
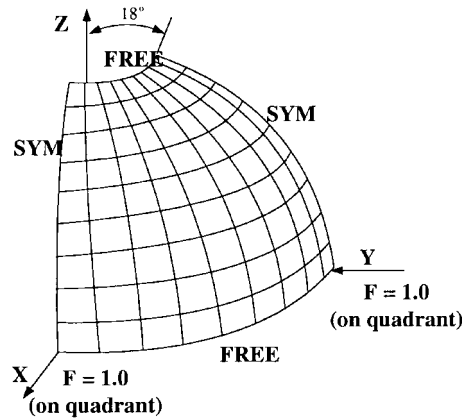

Fig. 4 Spherical shell, Radius = 10.0 : thickness = 0.04, $E = 6.825 \times 10^7$, $v = 0.22$; Mesh = $N \times N$, loading : concentrated forces
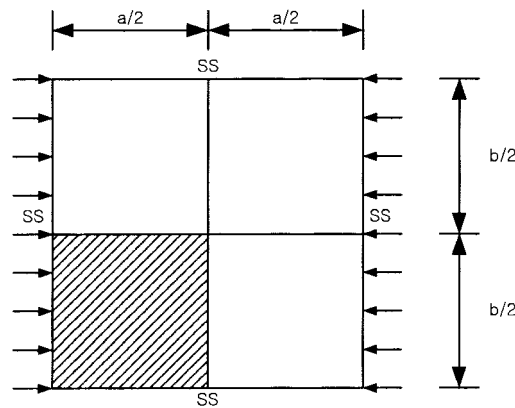

Fig. 5 Square plate under axial compression

Table 2 Hemispherical shell with 18 degree hole problem

QUAD8:Full [MacNeal]	QUAD8:Reduced [MacNeal]	QUAD8** [Lakshminaryana & Kailashi]	QUAD9** [Huang & Hinton]	XSHELL83 [XFINAS]
0.006 (4×4)	0.194 (4×4)	0.034 (2×2)	0.0863(2×2)	0.45(4×4)
0.069 (8×8)	0.895 (8×8)	0.383 (8×8)	0.538(4×4)	0.86(6×6)
0.210 (12×12)	1.005 (12×12)	0.765 (12×12)	0.948(8×8)	0.97(8×8)
0.373 (16×16)	1.008 (16×16)	0.940(16×16)		0.99 (10×10)

at the loading point given by MacNeal and Harder (1985) is 0.094. As noted for this problem, the membrane locking is more severe than the shear locking. This problem is a challenging test to the ability of a shell element to overcome membrane locking over most of the shell. Because of the symmetry, only one quadrant of the problem is modeled. In contrast to poor performance of the NASTRAN QUAD8 using full integration, the solution using reduced integration has better performance, but shows convergence over the unit value. The comparison of the normalized displacement of the SHELL8* solution with the solution given by in the references shows that the XSHELL83 formulation performs better than the others.

12.2 Buckling analysis of a simply supported plate under axial compression

In order to demonstrate the performance of the geometric stiffness formulation in this paper, a one-quarter of simply supported square plate shown in Fig. 5 was considered for the analysis of the elastic linear critical load. The 8-node shell element with 4×4 finite element mesh was used for the computation. The dimensions and the material properties were the length $a = 100$ mm, width of the loading side $b = 100$ mm, thickness $t = 1$ mm, modulus of elasticity $E = 30.0 \times 10^{06}$ N/mm^2 and Poisson's ratio $v = 0.3$. The critical bucking load obtained was compared with the theoretical non-dimensional factor $k = P_{cri}/(\pi^2 D/b^2)$ given in Timoshenko and Gere (1961), where $D = Et^3/(12(1 - v^2))$. The theoretical value of k for the plate model used is 4.0, while numerical value obtained using XFINAS for k was 3.9965, with an accuracy of 0.0875%. Both eigen solvers, the subspace iteration and the Lancsoz vector algorithm gave the same eigenvalue of 0.135454E04. This shows that the developed shell element based on the assumed strain method is robust and accurate in calculation buckling modes. In addition, the Lanczos vector algorithm recently successfully developed and tested in AIT shows computationally very efficient and accurate in solving critical buckling and free vibration problems. The use of the computationally efficient Lanczos vector algorithm in solving buckling problems of shell structures encourages in depth research on shell structures using the finite element method, since it reduces considerable amount of computational time and gives an equal accuracy as subspace iteration method by Kim *et al.* (2001).

12.3 Snap-through behaviour of curved panels under point loading

The class of test problems involves a structure susceptible to snap through behavior was investigated by Sabir and Lock (1973), and many references. In order to compare the results with references, non-linear analyses of hinged curved panels under central point loading were carried out. A symmetric quarter is modeled with a 4×4 shell element. The geometry and boundary conditions

are shown in Fig. 6 and material of shell was assumed to be linear elastic and isotropic. The results of load and deflection are plotted in Fig. 6. The result appears to be very consistent with reference to theory by Sabir and Lock up to the limit load. However, minor differences were observed but overall agreement is good. The solution strategy is based on XFINAS package which is suitable for instability analysis of steel shells.

12.4 Large deflection of elasto-plastic analysis of an imperfect plate under axial compression

The rectangular plate under axial compression was studied by Javaherian and Dowling (1985) using finite element methods. In this work large deflection and plasticity were incorporated. The imperfection shape has equivalent to $W = 0.001b\sin(\pi x/a)\sin(\pi y/b)$ in out-of-deflection.

The material and geometric data used are

$$a/b = 0.875, \quad b/t = 80, \quad t = 0.003175 \text{ m}, \quad E = 2.062 \times 10^{11}, \quad v = 0.3, \quad \sigma_Y = 2.5 \times 10^8 \text{ N/mm}^2$$

Two types of the results of the average stresses with average strain and out-of-plane deflection at the center of the plate are presented in Fig. 7. The curve of large deflection with plasticity tends to deflect downwards indicating that some unloading is taking place. The present result of large deflection and elasto-plastic analysis shows good agreement with references but solution by geometrical non-linearity shows some discrepancy after limit point.

12.5 Large deflection of elasto-plastic buckling of stiffened plate under axial compression

The present assumed strain element with six degrees of freedom would allow the stiffened plate

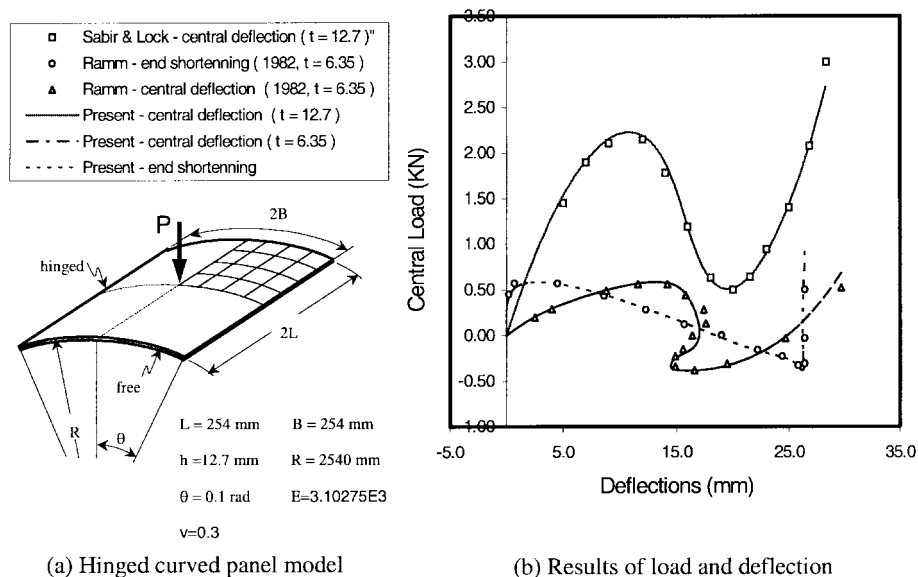(a) Hinged curved panel model   (b) Results of load and deflection
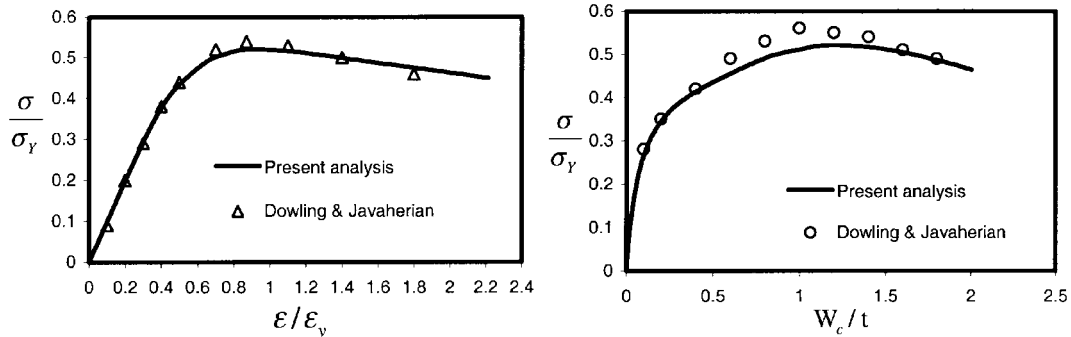
Fig. 6 Hinged cylindrical shell

Fig. 7 (a) Large deflection elastoplastic analysis of unstiffened thin shell (average stress vs. strain), (b) Large deflection elastoplastic analysis of unstiffened shell (average stress vs. center deflection)
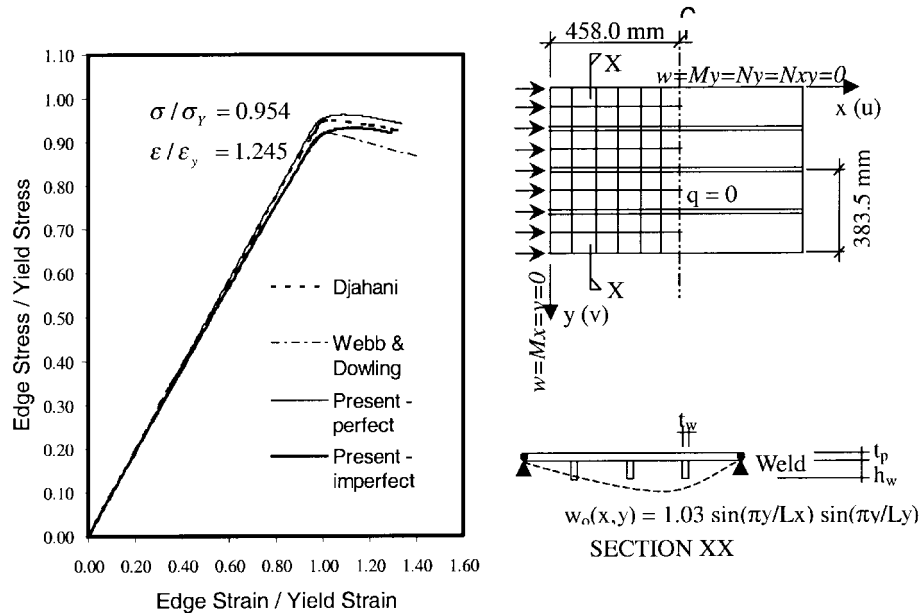

Fig. 8 Large deflection elastoplastic behaviour of discretely stiffened plates ($tp = 5.73$ mm, $hw = 60.3$ mm, $tw = 6.03$ mm, $\sigma o = 348$ N/mm^2, $E = 205000$ N/mm^2, $v = 0.3$)

and shell with complicated boundary condition. In the following the example of the eccentrically stiffened plate under the in-plane loading in Fig. 8 is presented by the large deflection of elasto-plastic analysis. The present results were compared with results by Web and Dowling (1980) and Dajahni (1977). The solution by Web and Dowling is based on the finite difference method incorporated with material and geometric non-linearity. They used the Ilyusin yield criteria for the plate plasticity and multi-layer approach for stiffener plasticity.

In Fig. 8, test result in reference by Web and Dowling (1980) is 0.835 and the predicted ultimate load is greater than that observed in the test. This is attributed to a difference between the actual and assumed residual stress. In general the load-shortening curves obtained showed good agreement

although there is discrepancy in the peak load. This is caused by different boundary condition applied along loaded edges by Web and Dowling (1980). In addition the effects of initial imperfection are investigated. As is shown in Fig. 7, the plate is less sensitive in initial imperfection than thin shell shown in next example.

12.6 Large deflection of elasto-plastic buckling analysis of stiffened cylindrical shells under axial compression

The example presented here is one of the interesting aspects, which shows the highly non-linear behaviour, i.e., snap back problem to test the capability of the non-linear shell element of stiffened shell. The model adopted is Agelidis (1984) panel widely used in Imperial College, London.

In order to get the local buckling mode shape of the stiffener, 2×6 shell elements shown in Fig. 9 were used in numerical modeling of cylindrical panel and stiffener. To specify the boundary condition efficiently, the local axes available in XFINAS were employed for assembling elements.

In order to identify the imperfection sensitivity of stringer stiffened shells under axial and pressure loading, Agelidis (1984) carried out a large parametric study of stiffened cylindrical shell covering a broad range of geometries used in the offshore structural engineering. The choice of a suitable imperfection shape is the most difficult task in the postbuckling analysis. One possible approach would be to select an imperfection mode related to the buckling mode obtained from linear eigenvalue analysis as well as a sine wave mode that is selected as a 'critical' imperfection mode. The other approach is to measure directly imperfections on panels followed by harmonic analysis or information available on characteristic models from imperfection databanks.

In this study, assuming an odd number of half waves for the deflection in the longitudinal direction only of the half panel between the rings was modeled. In the present study, it was decided to select imperfection shapes determined from a single half sine wave in circumferential and longitudinal directions. A further problem that had to be resolved is the determination of the maximum imperfection amplitude that can be allowed in the panel. It is, of course, inappropriate to use tolerance values from steel codes due to the entirely different manufacturing methods used in producing curved panels. The maximum amplitude in DNV used by Agelidis (1984) is adopted for the imperfection profiles.

As is shown in Fig. 10, small change of imperfection is very sensitive to the load carrying
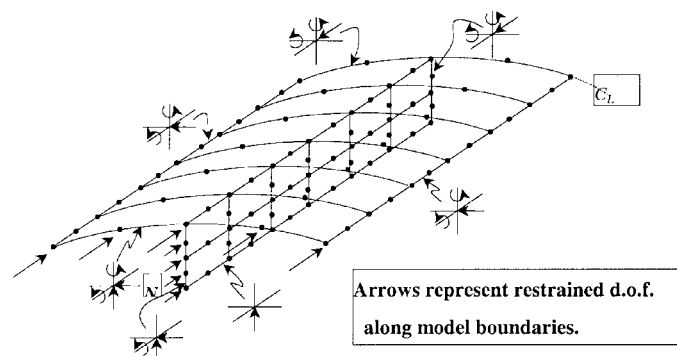

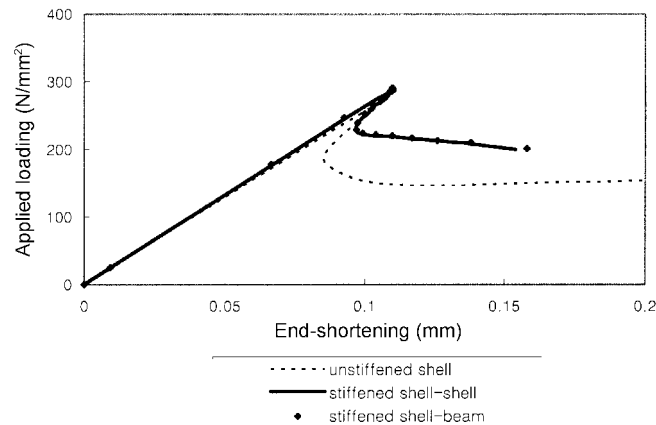Fig. 9 Stiffened shell under axial compression

Fig. 10 Load-deflection curve of stiffened curved panel

capacity. As expected, the curves showed unstable behavior after the limit load was attained, which is typical for wide panels. In general, imperfection sensitivity in a wide panel exhibiting cylinder-type behavior for which the knockdown factor for an imperfection amplitude is equal to 10% of the thickness is about 0.55. In this study the numerical 'knockdown' factor (defined here as the limit load obtained from non-linear analysis) is 0.51 for an imperfection amplitude equal to 10% of the thickness.

13. Conclusions

The non-linear buckling problems are presented to demonstrate the capability of the non-linear shell element. The present shell element formulation based on co-rotational assumed strain method overcomes the limit of thin plates and shells buckling problem. The tangent stiffness matrix which accounts for the resultant forces, moments and transverse shear forces is exactly defined on the midsurface of shell element by analytical integration. Thus, the present 8-nodes shell element is computationally efficient in the nonlinear analysis by ignoring numerical integration of the thickness direction and accurate. The results of elastoplastic buckling analyses showed good agreement in compared with references. The present shell element could be used in parametric study using proposed models in order to produce design guidance for stiffened plate and shell steel structures.

References

Agelidis, N. (1984), "Buckling of stringer stiffened shells under axial and pressure loading", Ph.D. Thesis, Dept. of Civil Engineering, Imperial College, London.

Ahmad, S., Irons, B.M. and Zienkiewicz, O.C. (1970), "Analysis of thick and thin shell structures by curved finite elements", *Int. J. Numer. Meth. Eng.*, **2**, 419-451.

Bates, D.N. (1987), "The mechanics of thin walled structures with special reference to finite rotations", Ph.D. Thesis, Dept. of Civil Engineering, Imperial College.

Bathe, K.J. and Dvorkin, E.N. (1986), "A formulation of general shell elements-The use of mixed interpolation of tensorial components", *Int. J. Numer. Meth. Engng.*, **22**, 697-722.

Betsch, P. and Stein, E. (1999), "Numerical implementation of multiplicative elasto-plasticity into assumed strain element with application to shell at large strains", *Compt. Methods Appli. Mech. Engrg.*, **179**, 215-245.

Belytschko, T. and Hsieh, B.J. (1973), "Non-linear transient finite element analysis with convected co-ordinates", *Int. J. Solids Structures*, **7**, 255-271.

Choi, C.K. and Yoo, S.W. (1991), "Geometrically nonlinear behaviour of an improved degenerated shell element", *Comput. Struct.*, **40**, 785-794.

Crisfield, M.A. (1981), "A fast incremental/iterative solution procedures that handles snap-through", *Comput. Struct.*, **13**, 55-62.

Djhani, P. (1977), "Large deflection elasto-plastic analysis of discretely stiffened plates", Ph.D. Thesis. Dept. of Civil Engineering, Imperial College, London.

FINASIC User Manual (1990), Dept. of Civil Engineering, Imperail College, London.

Huang, H.C. (1987), "Implementation of assumed strain degenerated shell elements", *Comput. Struct.*, **29**(1),147-155.

Huang, H.C. and Hinton, E. (1986), "A new nine node degenerated shell element with enhanced membrane and shear interpolation", *Int. J. Numer. Meth. Engng.*, **22**, 73-92.

Javaherian, H. and Dowling, P.J. (1985), "Large deflection elasto-plastic analysis of thin shells", *Engng. Struct.*, **7**, July, 154-162.

Kebari, H. and Cassel, A.C. (1992), "A stabilized 9-node non-linear shell element", *Int. J. Numer. Meth. Engng*, **35**, 37-61.

Kanok-Nukulchai, W. (1979), "A simple and efficient finite element for general shell analysis", *Int. J. Numer. Meth. Eng.*, **14**, 179-200.

Kim, K.D. and Voyiadjis, G.Z. (1999), "Non-linear finite element analysis of composite panels", *Composites Part B: Engineering*, **30**(4), 383-394.

Kim, K.D. (1992), "Non-linear analysis of fibre-reinforced composite structures using finite elements", Ph.D. Thesis , Dept. of Civil Engineering, Imperial College.

Kim, K.D., Park, T.Y. and Voyiadjis, G.Z. (1998), "Postbuckling, analysis of composite panels with imperfection damage", *Comput. Mech.*, **22**, 375-387.

Kim, K.D., Sunil Munasinghe, H.M. and Kanok-Nukulchai, W. (2001), "Buckling behaviour of cylindrical shell under axial compression using Lanczos vector", *The Eighth East Asia-Pacific Conference on Structural Engineering and Construction EASEC-8* : 5-7 December 2001.

Kim, K.D. and Park, T.H. (2001), "An 8-node assumed strain element with explicit integration for isotropic and laminated composite shells", *Struct. Eng. Mech.*, **13**(4), 387-410.

Lakshminaryana, H.V. and Kailashi, K. (1989), "A shear deforamble curved shell element of quadrilateral shape", *Comput. Struct.*, 987-1001.

MacNeal, R.H. and Harder, R.L. (1985), "A proposed standard set of problems to test finite element accuracy", *Finite Elements Analysis and Design*, **11**, 3-20.

Ramm, E. The Riks/Wempner (1982) "Approach-an extension of the displacement control method in nonlinear analysis", in *Recent Advances in Non-linear Computational Mechanics*, eds E. Hinton, D.R.J. Owen and C.Taylor, Pineridge Press, Swansea,U.K., 63-86.

Sabir, A.B. and Lock, A.C. (1973), "The application of finite elements to large deflection geometrically nonlinear behaviour of cylindrical shells", in *Variational Method in engineering*(Editor, Brebbia, C.A. and Totenham, H.N.) Southampton University Press, 7/66-7/75.

Yoo, S.W. and Choi, C.K. (2000), "Geometrically nonlinear analysis of laminated composite by an improved degenerated shell element", *Struct. Eng. Mech.*, **9**(1), 99-110.

Webb, S.E. and Dowling, P.J. (1980), "Large-deflection elasto-plastic behaviour of discretely stiffened plates", *Proceeding of Institutions of Civil Engineers*, Part 2, 69, 3 June 75-401.

Ziegler, H. (1968), *The Principle of Structural Stability*, Blaisdell Publishing Company.

Notations

–   : bar over : value measured at midsurface

x, y, z	: global coordinate system
r, s, t	: local coordinate system
ξ, η, ζ	: natural coordinate system
i	: superscript referring to node number i
m, b, q	: subscript referring to membrane, bending and transverse shear respectively
P	: position vector
H^i	: shape function at node i
T	: direction cosine of the new local axes with respect to the global axes
$\overline{U} = (\overline{U}, \overline{V}, \overline{W})$	: global translation of the midsurface
$\theta = (\theta_x, \theta_y, \theta_z)$	: global rotation of the midsurface
$\overline{u} = (\overline{u}, \overline{v}, \overline{w})$	: local translation of the midsurface
$\varphi = (\varphi_r, \varphi_s, \varphi_t)$	: local rotation of the midsurface
$U = (\overline{U}, \theta)$	: global displacement
$u = (\overline{u}, \varphi)$	: local displacement
V_r, V_s, V_t	: base vector tangential to the local co-ordinates
e_m, e_b, e_q	: linear part of the membrane, bending and transverse shear strain vector
$\gamma_{\xi\zeta}, \gamma_{\eta\zeta}$	: transverse shear strains in the natural coordinates
N, M, Q	: resultant membrane forces (N_r, N_s, N_{rs}), moments (M_r, M_s, M_{rs}), and transverse shear forces (Q_r, Q_s)
$\overline{\sigma}$	: effective stress
σ_Y	: current uni-axial yield stress
$\overline{h}$	: hardening parameter
f	: low vector